Korean J. Chem. Eng., 39(8), 2192-2200 (2022)
DOI: 10.1007/s11814-021-1055-2

pISSN: 0256-1115
eISSN: 1975-7220

Differential pulse voltammetric sensor for tetracycline using manganese tungstate nanowafers and functionalized carbon nanofiber modified electrode

Ramya Ramkumar, Ganesh Dhakal, Jae-Jin Shim, and Woo Kyoung Kim†

School of Chemical Engineering, Yeungnam University, Gyeongsan, Gyeongbuk 38541, Korea
(*Received 16 November 2021 • Revised 15 December 2021 • Accepted 29 December 2021*)

Abstract−A label-free approach was employed to selectively detect tetracycline using manganese tungstate ($MnWO_4$) nanowafers and functionalized carbon nanofiber-modified glassy carbon electrode (GCE). $MnWO_4$ nanowafers were synthesized hydrothermally and characterized along with functionalized carbon nanofibers (f-CNFs). Cyclic voltammetry and differential pulse voltammetry were employed to detect tetracycline, and the sensor exhibited linear ranges of detection of 1.75−109.25 μM and 109.25−409.25 μM, respectively. The limit of detection was found to be 0.24 μM (S/N=3) with a sensitivity of 9.91 μA μM^{-1} cm^{-2}. Interference studies were carried out with ciprofloxacin (Cip), penicillin (Pen), and amoxicillin (Amox). The modified electrode ($MnWO_4$/f-CNF/GCE) was found to provide sensitive and selective detection of tetracycline in the presence of interfering agents.

Keywords: Manganese Tungstate, Nanowafers, Carbon Nanofibers, Tetracycline, Sensor, Interference

INTRODUCTION

Tetracyclines are a group of antibiotics used to treat bacterial infections in animals, owing to their low cost and broader spectrum of activity. However, their increased use has caused trace levels in human foodstuffs that pose several health threats. Also, the widespread usage has led to severe bacterial resistance in animals and humans [1]. Yet, in spite of its drawbacks, tetracycline is preferred widely over its counterparts because of its low toxicity, low production cost, minimal side effects, and easy oral absorption [2]. The inhibitory concentration of tetracycline in human blood serum and urine is known to be ~0.5 μg mL^{-1} [3]; hence, selective and sensitive detection is imperative. Because of its immunomodulatory properties, tetracycline is used with steroids to treat systemic and local bacterial infections in animals and aquaculture. Studies have shown that compared with oxytetracycline, tetracycline is excreted more slowly in the urine [4]; hence, its detection in minute quantities is necessary.

The active materials employed in this study, namely $MnWO_4$ and functionalized carbon nanofibers (f-CNFs), are used in several interesting applications. Metal oxides are important candidates for various applications, including catalysis, adsorbents, superconductors, semiconductors, functional ceramics, and antifungal treatment. Among the metal oxides, manganese-tungstate-based materials have been extensively used in energy and catalytic applications because of their photoluminescence and redox properties [5]. $MnWO_4$ has been used mainly as an active material for energy storage, and a few studies have demonstrated its photocatalytic activity [6], effectiveness for sensing heavy metal ions [7], oxidation of short-chain alkanes [5], and bio-imaging [8]. Carbon based materials have found unparalleled usage in many industries due to their unique properties and advantages, including good electrical conductivity, high surface area, fast electron transfer rates, and good electrochemical windows. Carbon nanofibers, particularly f-CNF, are emerging compounds with high aspect ratio, high strength, low density, metallic conductivity, and good chemical and environmental stability [9]. Carbon nanofibers have been employed in various applications, including supercapacitors [10], biosensors [11], water treatment [12], and hydrogen storage [13].

As summarized in Table 1, several approaches have been employed in modified electrodes, such as metal nanoparticles [14], conducting polymers [15], carbon [16], and quantum dots [17], for sensing tetracycline; however, in most studies, sensing was performed in acidic pH. The modified electrode developed herein functions optimally at neutral pH. Many researchers have used aptamers to detect tetracycline and have achieved very low detection limits and wide linear ranges with reasonable sensitivities. In general, aptamer-based sensors suffer from nuclease degradation and poor serum stability in biological media (blood and serum); thus, it is challenging to employ such sensors in real-time medical applications. Using noble metals for detecting tetracyclines also has disadvantages because of their high cost and tedious electrode preparation.

In this study, we employed a label-free sensor using hydrothermally synthesized manganese tungstate nanowafers with a glassy carbon electrode (GCE) modified with functionalized carbon nanofibers. The sensor can effectively detect tetracycline at micromolar levels (low detection limit of 0.24 μM) using differential pulse voltammetry (DPV). Sensitive techniques such as DPV were utilized to ascertain the effect of current and other parameters for the detection of tetracycline. DPV is preferred over cyclic voltammetry (CV) and linear sweep voltammetry (LSV) because of its selectivity towards redox processes [18]. $MnWO_4$ can be synthesized from cost-effective precursors using a hydrothermal process and can be em-

†To whom correspondence should be addressed.
E-mail: wkim@ynu.ac.kr

Table 1. Analytical parameters of reported systems for tetracycline detection

Modified electrode	Method	Linear range (μM)	LOD (μM)	Reference
PtNPs/C/GCE	CV	9.99-44.0	4.28	[14]
MWNTs-GNPs/MIP/GCE	CV	2-90	0.09	[15]
MIOPPy-AuNP/SPCE	DPV	1-20	0.65	[30]
Anti-TET/PGA/MWCNTs/GCE	EIS	$1*10^{-10}$-1	$3.7*10^{-11}$	[32]
Au/g-C_3N_4/GCE	CV	1-20 20-200	0.03	[33]
Biotinylated-ssDNA/Streptavidin/SPAuE	SWV	0.01-10	0.01	[34]
MWCNTs-COOH/GO/CPE	AdSDPV	20-3100	0.36	[35]
FeZn/MMT/GCE	DPV	0.3-52	0.10	[36]
GCE-Gr-AuNP	CA	2.9-153	16.2	[37]
BNQDs	Fluorescence	0-1 2.5-50	0.019	[38]
Ag@SiO_2/CdTeQDs-DNA-Aptamer	Fluorescence	0.2-400	0.016	[39]
CuCDs	Fluorescence	2-32	0.17	[40]
AgNCs	Fluorescence	1.12-230	0.47	[41]
$MnWO_4$/f-CNF/GCE	DPV	1.75-409.25	0.24	This Work

*LOD-limit of detection, DPV-differential pulse voltammetry, PtNP-platinum nanoparticles, C-carbon, MIOPPy-molecularly imprinted overoxidized polypyrrole, PGA-poly(L-glutamic acid), MIP-molecularly imprinted polymer, MWCNT-multiwalled carbon nanotubes, GNP-gold nanoparticle, CV-cyclic voltammetry, CNF-carbon nanofibers, SPAuE-screen printed gold electrode, SWV-square wave voltammetry, PtNPs/C-platinum nanoparticles/Carbon, COOH-MWCNTs-carboxyl functionalized multiwalled carbon nanotubes, CS-complementary strands, GR-SPCE-graphene screen printed carbon electrode, GO-graphene oxide, AdSDPV-adsorptive stripping differential pulse voltammetry, FeZn/MMT/GCE-IronZinc/montmorillonite/glassy carbon electrode, CA-Chronoamperometry, BNQDs-boron nitride quantum dots, Ag@SiO_2/CdTeQDs-silver@silicondioxide/cadmiumtellurium Quantum dots, CuCDs-copper doped carbon dots, AgNCs-silver nanoclusters.

ployed without any further additives, decoration, or processing. The active materials, i.e., $MnWO_4$ nanowafers, were initially tested with many analytes for sensor applications. With tetracycline the active material produced two sensitive and selective peaks in DPV analysis and hence was chosen to study the detection of tetracycline on glassy carbon electrodes. $MnWO_4$ is an electrochemically active material with excellent redox properties. This is the first study to employ $MnWO_4$ as a sensor electrode for detecting a potentially important drug - tetracycline. Sensitive techniques such as DPV were utilized to ascertain the effect of current and other parameters for the detection of tetracycline. The developed sensor performs best at neutral pH, a favorable condition for detecting analytes in biological media. Also, the sensor is effective against potential interferents like ciprofloxacin, penicillin and amoxicillin.

MATERIALS AND METHODS

1. Reagents

Manganese(II) acetate tetrahydrate ($C_4H_6MnO_4{\cdot}4H_2O$), sodium tungstate (Na_2WO_4), and carbon nanofibers (CNFs) were purchased from Sigma Aldrich. Ethylene glycol, tetracycline, penicillin, ciprofloxacin, amoxicillin, ethanol, sulfuric acid, nitric acid, and hydrochloric acid were purchased from Merck Chemicals. All the chemicals were of analytical grade and were used as received. Because tetracycline undergoes photolytic degradation [19], the antibiotic solutions were prepared right before each experiment. Phosphate-buffered saline (PBS) buffers were prepared using sodium hydrogen phosphate, potassium dihydrogen phosphate, sodium chloride, and potassium chloride, all obtained from Merck Chemicals. All the solutions were prepared using deionized (DI) water, and all the experiments were carried out at room temperature (25±1 °C).

2. Electrode Materials Synthesis

The hydrothermal method was employed to synthesize the precursor ($MnWO_4$) from the starting materials, manganese(II) acetate tetrahydrate and sodium tungstate [20]. A 50 mM solution was prepared by dissolving 0.61 g of $C_4H_6MnO_4{\cdot}4H_2O$ in ethylene glycol (50 mL) and stirring the solution continuously for 30 min. Thereafter, 0.82 g of sodium tungstate was added to the above solution and stirred again for 30 min at room temperature. This mixture was then transferred to an autoclave and heated at 150 °C for 12 h. The resultant material was washed with an equal volume of ethanol and water and thermally annealed at 500 °C for 4 h. Functionalized CNFs were prepared using CNF obtained from Sigma Aldrich. CNF (1 g) was dispersed in a mixture of nitric and sulfuric acid (1 : 3). This mixture was refluxed at 60 °C for 12 h, washed with water, and then with acetone and ethanol. The resultant functionalized CNFs were dried and kept in a vacuum oven at 60 °C until further use.

3. Electrochemical Studies

All the electrochemical studies, including cyclic voltammetry (CV), amperometry, and DPV, were performed using an Autolab PGSTAT302N (Metrohm, Netherlands). The working electrode was a modified GCE (3 mm, CH Instruments, USA), while the reference electrode was a saturated calomel electrode (SCE). A Pt wire was used as the counter electrode (CH Instruments, USA) in a three-electrode arrangement. The GCE was polished with 0.50 and 0.03

μm alumina powder on microcloth pads, cleaned with ethanol and DI water several times, and dried by purging with nitrogen for 30 min before each use. The working electrode was modified with $MnWO_4$/f-CNF for the detection of tetracycline in all the measurements and is denoted as $MnWO_4$/f-CNF/GCE. All the reported potentials are vs. SCE.

4. Electrochemical Sensor Construction

The preparation of the GCE is crucial to achieve good sensitivity, stability, and reproducibility of the sensor. After the pretreatment, the GCE was modified with a slurry of $MnWO_4$ and f-CNF in 1 : 1, 1 : 2, and 1 : 3 ratios (w/w) in DI water. Various loadings (2-10 μL) of this slurry were drop-cast onto the GCE. The slurry, composed of 2-10 mg $MnWO_4$ and 1-10 mg f-CNF, was sonicated for 30 min to obtain uniform dispersion. The modified electrode was dried at 60 °C in a vacuum oven for 10 min and stored in a desiccator before use.

5. Sensor Optimization

The sensor performance was optimized by varying several parameters, such as the concentrations of starting materials and their ratios and pH. In the DPV measurements, the pulse width, pulse amplitude, scan rate, and other parameters were varied to study their effect on the performance of the sensor. In the chronoamperometric measurements, the potential was varied from 0.4 V to 0.7 V to study its effect on the performance of the sensor and to find the optimum current for tetracycline detection.

RESULTS AND DISCUSSION

1. Electrode Materials Characterization

$MnWO_4$, synthesized by the hydrothermal process, and f-CNF were characterized using scanning electron microscopy (SEM), Fourier-transform infrared (FTIR) spectroscopy, and X-ray diffraction (XRD). The SEM images (Fig. 1) confirm the nanowafer-like morphology of $MnWO_4$ (Fig. 1(a)) and the mixed fiber and tubular morphology of the f-CNFs (Fig. 1(b)) and $MnWO_4$/f-CNF composite (Fig. 1(c)). Additional SEM images at higher magnification are shown in Fig. S1 in the Supplementary Information (SI). The SEM images of the composite show that the structure of the starting materials remained intact when mixed and sonicated into a slurry at different $MnWO_4$ and f-CNF ratios (1 : 1, 1 : 2, and 1 : 3). The SEM images of $MnWO_4$ show a porous structure and flake-like nanowafers with wall thicknesses of 20-30 nm. The nanowafers comprised a network of nanoparticles. The f-CNFs exhibited an overlapped and highly elongated fiber-like morphology. The length of the fibers ranged from a few nanometers to several micrometers, and their diameter ranged from 50 to 120 nm. The particles of the $MnWO_4$/f-CNF composite, as seen in Fig. 1(c), were well dispersed, showing the same structure and morphology as the starting materials ($MnWO_4$ and f-CNF). The structural integrity was clearly maintained, facilitating the detection of the antibiotic (tetracycline) with good sensitivity.

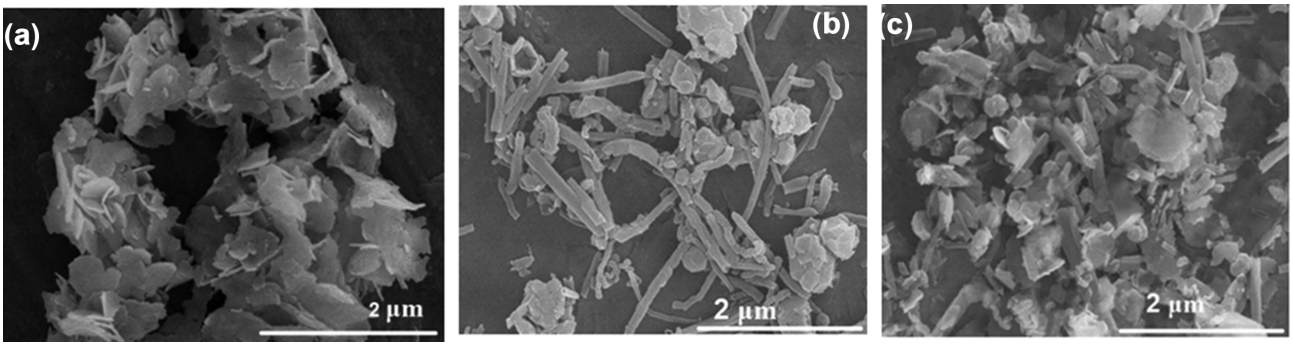

Fig. 1. SEM images of (a) $MnWO_4$, (b) f-CNF, and (c) $MnWO_4$/f-CNF composite at 25 k magnification.

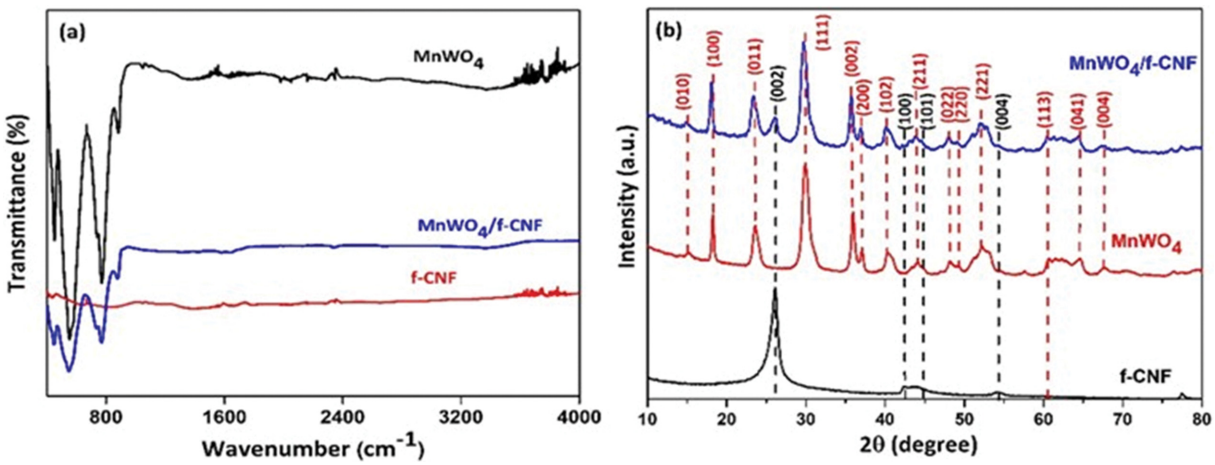

Fig. 2. (a) FTIR and (b) XRD patterns of $MnWO_4$ and f-CNF samples.

The FTIR spectra in Fig. 2(a) show the vibrations of $MnWO_4$, f-CNF and the composite. All the peaks in the FTIR spectra in the mid-infrared region corresponding to low frequencies are sharp and clear. The broad band obtained near 3,500-3,200 cm^{-1} indicates the vibration of the O-H bond in the surface-hydrated $MnWO_4$. Weak bands were also observed at 1,637 cm^{-1}, corresponding to the H-O-H deformation vibration of the surface hydroxyl group. The sharp peaks observed at 883 and 772 cm^{-1} indicate the symmetric and asymmetric stretching vibrations of the short bond of the W-O moiety present in the terminal WO_2 groups. The vibrations at 740 and 578 cm^{-1} were assigned to the asymmetric stretching vibrations of the longer W-O bond in the W_2O_4 chain. The in-plane deformation modes of the longer W-O bonds are indicated by the peaks at 459 and 552 cm^{-1}. The band at 428 cm^{-1} can be assigned to the in-plane deformation vibrational modes of the W-O bond in the terminal WO_2 groups [21]. The FTIR spectrum of f-CNF is shown in Fig. 2(a). For the acid-treated f-CNF, strong vibration peaks were observed at 1,782 cm^{-1}, corresponding to the C=O stretching of the acid carbonyl group. The broad peak around 3,300 cm^{-1} corresponds to the vibration of the O-H bonds from surface hydration. The peak at 1,647 cm^{-1} corresponds to adsorbed water molecules on the surface. The peak at 2,969 cm^{-1} indicates CH stretching vibration, and the peak at 1,381 cm^{-1} is derived from -CH bending vibration. The peak at 1,049 cm^{-1} indicates the C-O-C stretching of the acid functionality on the f-CNF, and the peak at 878 cm^{-1} belongs to the anomeric vibration of carbon [22]. Fig. 2(a) shows all of the above peaks for f-CNF. The FTIR spectra of $MnWO_4$/f-CNF contained all the peaks corresponding to the vibration of $MnWO_4$ and f-CNF, respectively.

The information obtained from the XRD studies showed the crystalline structure, phase purity, and grain size of $MnWO_4$ synthesized by the hydrothermal method. The XRD pattern of $MnWO_4$ is shown in Fig. 2(b). Several sharp peaks indicate the crystalline nature of the $MnWO_4$ nanowafers. The peaks at 2θ=15.2°, 18.3°, 23.6°, 29.9°, 35.9°, 37.1°, 40.4°, 44.1°, 48.2°, 49.3°, 53.2°, 60.7°, 64.5°, and 67.6° correspond to the (010), (100), (011), (111), (002), (200), (102), (211), (022), (220), (221), (113), (041), and (004) crystal planes of $MnWO_4$, respectively. The lattice parameters deduced from the Debye Scherrer formula suggest a monoclinic structure with an average grain size of 9.4 nm. Fig. 2(b) also shows the XRD pattern of the acid-functionalized CNF, in which the sharp peaks at 26.1°, 42.5°, 44.1°, and 54.3° correspond to the (002), (100), (101), and (004) planes, respectively [23]. The calculated structural parameters matched well with the JCPDS card number (80-0133) for $MnWO_4$. The XRD pattern of the $MnWO_4$/f-CNF showed all the peaks corresponding to $MnWO_4$ and showed a more pronounced

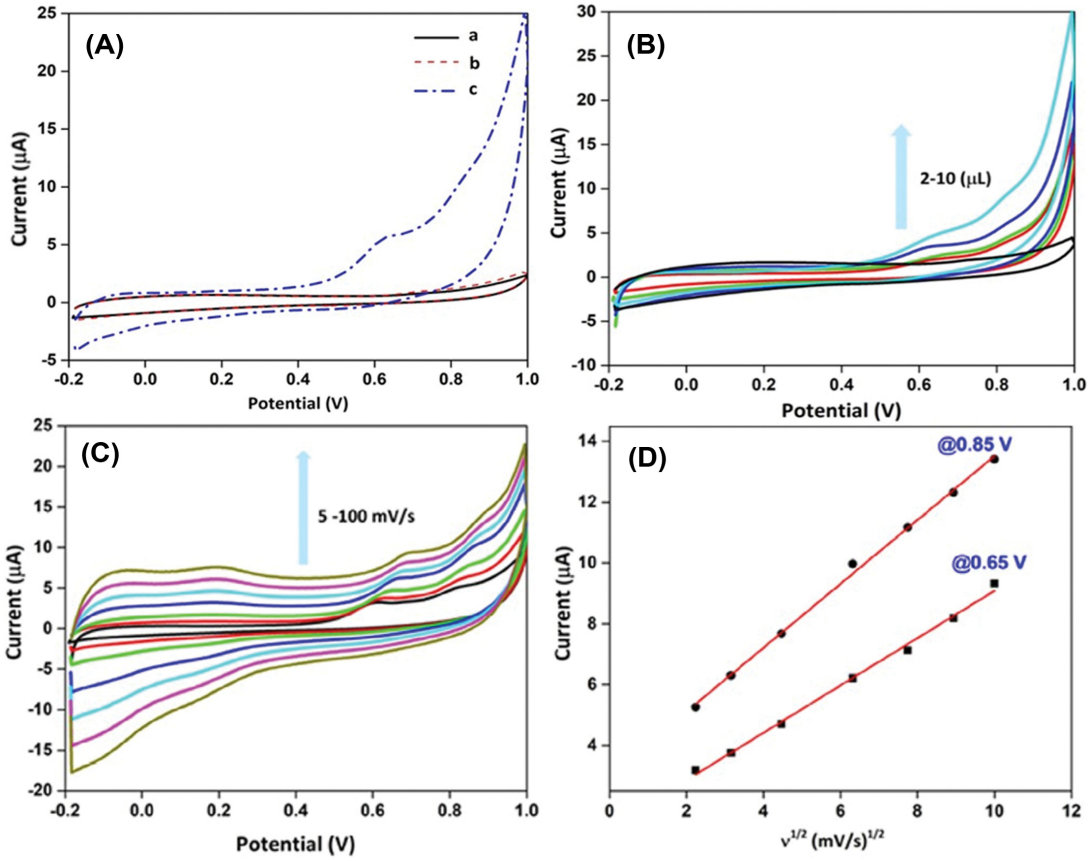

Fig. 3. (A) CV's of (a) bare GCE, (b) $MnWO_4$-modified GCE, and (c) $MnWO_4$/f-CNF/GCE-modified electrode in the presence of 100 μM tetracycline, (B) CV's of $MnWO_4$/f-CNF/GCE electrode with various loadings from 2 to 10 μg mL^{-1} in the presence of 100 μM tetracycline. The $MnWO_4$: f-CNF weight ratio is 1 : 2. (C) CV's of $MnWO_4$/f-CNF/GCE modified electrode at scan rates from 5 to 100 mV s^{-1} in the presence of 100 μM tetracycline, and (D) peak current vs. square root of scan rate at 0.65 V and 0.85 V.

peak at 2θ=26.1°, corresponding to the f-CNF moiety.

2. CV Measurements

Fig. 3(A) shows the cyclic voltammograms of the bare GCE, $MnWO_4$/GCE, and the composite $MnWO_4$/f-CNF/GCE in the potential window from −0.2 to 1.0 V, all acquired at a scan rate of 10 mV s^{-1} in the presence of 100 μM tetracycline in PBS 7 buffer as the electrolyte. All cyclic voltammetry experiments were carried out after 20 cycles at 40 mV s^{-1} in PBS (pH 7) to stabilize the current response, as shown in Fig. S2(SI). The current response for the oxidation of tetracycline on the modified electrode was nearly ten times greater than that of the bare GCE and $MnWO_4$-modified electrodes. The composite showed higher activity than that of the bare GCE and $MnWO_4$-modified electrode, indicating its suitability as a sensor. The sensor was tested for various loadings of the active material by CV analysis and the results are shown in Fig 3(B) and explained in detail in the "Effect of loading" section. The effect of the tetracycline concentration on its detection by the $MnWO_4$/f-CNF/GCE-modified electrode was studied by CV, and the results are presented in Fig. S3(SI). The results show that the current response increased almost monotonically with the tetracycline concentration. The CV results show two faint peaks corresponding to the oxidation of tetracycline at 0.65 V and 0.85 V. The scan-rate dependence of the composite electrode was studied from 5 to 100 mV s^{-1} in the presence of 100 μM tetracycline in 0.1 mM PBS 7 buffer, and the results are shown in Fig. 3(C). The cyclic voltammograms are influenced by diffusion-limited and kinetically controlled processes. If a redox process is solely influenced by diffusion, the peak potential will be generally independent of the scan rate. On the other hand, if the electrode kinetics plays a predominant role, the scan rate affects the entire voltammetric response, in particular, the location of the peak potential. We plotted the current vs. square root of scan rate for tetracycline oxidation, and this reaction seems to be quasi-reversible in relation to the oxidation of tetracycline. But the $MnWO_4$ as a redox active material exhibits redox peaks in the CV results. The peak current vs. square root of the scan rate plots displayed in Fig. 3(D) shows the linear relationship expected for diffusion controlled processes [24], indicating the oxidation of tetracycline is diffusion-controlled at the modified electrodes. The peak potentials shifted to more positive values with increasing scan rate, but unlike other systems reported in the literature [25], the peaks remained sharp at all scan rates and were not broadened. For consistency in the measurements, a scan rate of 10 mV s^{-1} was selected for all CV measurements. Two characteristic peaks were observed at 0.65 and at 0.85 V (vs. SCE), corresponding to the oxidation of tetracycline. Related studies by Calixto et al. (at pH 7) [26] agree well with this finding. The oxidation peak at 0.65 V corresponds to the conversion of the phenolic moiety to a benzoquinone moiety, and the oxidation peak at 0.85 V corresponds to the conversion of the dimethylamine moiety to N-dimethylated products, which in turn corresponds to the adsorption peak observed for the composite electrode [27]. The peak position for the oxidation of tetracycline using the $MnWO_4$/f-CNF modified electrode with an electrolyte at pH 7 represents a significant shift to a lower pH. This is significant because the oxidation of tetracycline mainly occurs at acidic pH and only a few papers have reported tetracycline oxidation at neutral pH. It suggests that it is possible to analyze tetracycline in biological samples which exists in neutral pH values. Furthermore, the modified electrode exhibited a reversible peak due to the oxidation of $MnWO_4$ at 0.15 V at higher scan rates and at neutral pH [28]. Pseudocapacitive behavior was also observed at high scan rates, indicating the suitability of this modified electrode for energy storage applications.

3. Effect of $MnWO_4$ and f-CNF Loading

As shown in Fig. 3(B), the effect of various precursor ($MnWO_4$ and f-CNF) loadings on the modified GCE was investigated in the presence of 100 μM tetracycline in 0.1% buffer (pH 7). $MnWO_4$ to f-CNF ratios of 1 : 1, 1 : 2, and 1 : 3 were used. A slurry of each mixture was suspended in 1 mL of DI water and ultrasonicated for 1 h. The slurry with various loadings was drop-cast onto the GCE electrode and subsequently dried at 60 °C for 10 min. The optimum ratio of the precursor was 1 : 2 ($MnWO_4$: f-CNF). As the loading of $MnWO_4$: f-CNF (1 : 2) increased from 2 to 10 μg mL^{-1}, the oxidation current of tetracycline also increased. However, at 10 μg mL^{-1}, the electrode was completely covered, and some

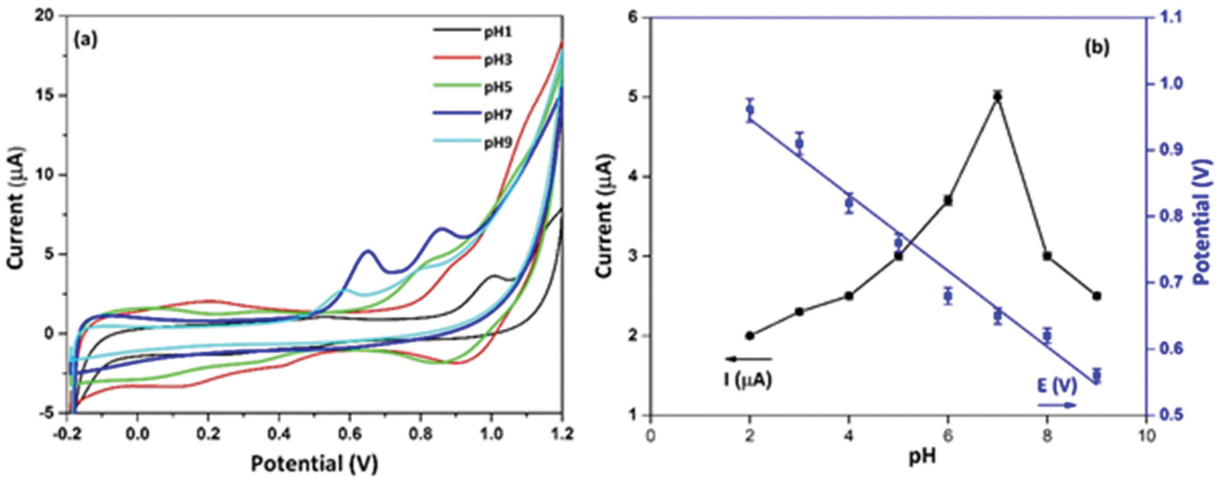

Fig. 4. (a) CV's of $MnWO_4$/f-CNF/GCE in the presence of different pH (1, 3, 4, 7 and 9), and (b) dependence of peak potential and peak current on pH using $MnWO_4$/f-CNF/GCE-modified electrode in the presence of 100 μM tetracycline.

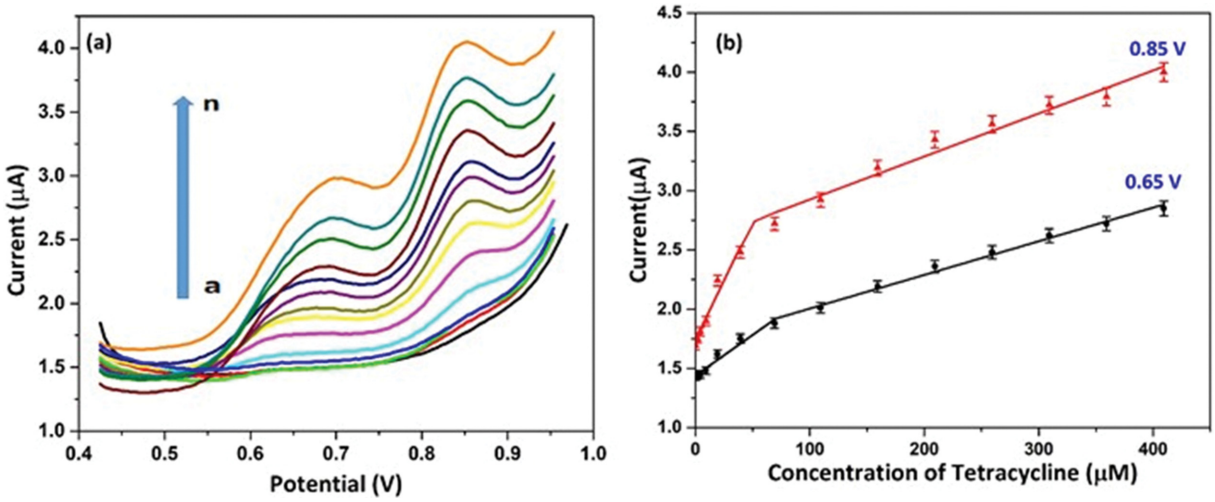

Fig. 5. (a) Differential pulse voltammograms of $MnWO_4$/f-CNF/GCE-modified electrode in the presence of different concentrations of tetracycline [a] 0, [b] 1.75, [c] 4.25, [d] 9.25, [e] 19.25, [f] 39.25, [g] 69.25, [h] 109.25, [i] 159.25, [j] 209.25, [k] 259.25, [l] 309.25, [m] 359.25, and [n] 409.25 μM, (b) corresponding calibration curves at 0.65 V and 0.85 V.

active material (composite) was found on the Teflon lining of the GCE. Furthermore, the oxidation peaks of tetracycline were distinct, with high peak currents at a loading of 8 μg mL^{-1}. Hence, 8 μg mL^{-1} was selected as the optimum loading for the detection of tetracycline.

4. Effect of pH

Fig. 4(a) and (b) shows the effect of pH, in the range of 1-9, on the detection of tetracycline using the modified GC electrode in 0.1 mM PBS solutions. No binder was used for the modified electrodes, and the results were obtained using the as-prepared electrode at various pH values. The peak potential and the corresponding peak current were plotted against the pH [29]. The results suggest that the peak potentials corresponding to the characteristic current peak decreased monotonically with increasing pH (pH 1 to pH 9), suggesting the involvement of protons in this reaction. The involvement of protons in the reaction is indicated by shift in the redox peak potential with pH. In this case, the peak potential shifted to more negative values with increasing pH (i.e., from 1 to 9). This indicated that the solution pH and the tetracycline oxidation were linearly proportional at pH range 1 to 9, also denoting the involvement of protons in the reaction. Another factor which confirms the above fact is the increasing oxidation peak current from pH 1 to 7, reaching a maximum at pH 7 and then decreasing after pH 7. Also the physiological pH is pH 7, at which most of the interferents can also be successfully excluded in the determination of tetracycline. In the pH 7 buffer, the composite electrode exhibited clear peaks of tetracycline oxidation at 0.65 V and 0.85 V (as shown in Fig. 3); hence, the medium at pH 7 was chosen for the detection of tetracycline in all further studies.

5. DPV Measurements

DPV was employed for rapid tetracycline sensing using the electrode in 0.1 M PBS (pH 7). As shown in Fig. S4, the DPV curves were recorded at different pulse amplitudes to assess tetracycline sensing sensitivity. The optimum pulse amplitude was chosen as 25 mV and the scan rate was 10 or 50 mV s^{-1}; these values were employed for the rest of the DPV measurements.

Tetracycline was added to the PBS solution in increasing concentrations from 1.75 to 409.25 μM, and the DPV curves were recorded, as shown in Fig. 5(a); the peak current vs. tetracycline concentration plot is shown in Fig. 5(b). From the DPV curves, it is evident that as the concentration of tetracycline increased, the current increased, indicating the oxidation of tetracycline on the $MnWO_4$/f-CNF/GCE electrode. Two linear ranges were observed in the DPV curves, as shown in Fig. 5(b). The regression equation for the first linear range corresponding to the low concentration range of 1.75-59.25 μM at 0.65 V (the first oxidation peak for tetracycline) is represented as $I_{(0.65\,V)}$ (μA)=0.007 C_{Tet}+1.438 with a correlation coefficient (R^2) of 0.97. The regression equation at 0.85 V (corresponding to the second oxidation peak for tetracycline) is $I_{(0.85\,V)}$ (μA)=0.015 C_{Tet}+1.774, with R^2=0.96. The second linear range observed from the DPV curves corresponds to a concentration range of 59.25-409.25 μM. The regression equation at 0.65 V is represented as $I_{(0.65\,V)}$ (μA)=0.003 C_{Tet}+1.637, with R^2=0.99, and the linear regression equation at 0.85 V is $I_{(0.85\,V)}$ (μA)=0.004 C_{Tet}+2.402, with R^2=0.97. The limit of detection (LOD) for tetracycline, determined from the DPV curves, is 0.24 μM, with a sensitivity of 9.91 μA μM^{-1} cm^{-2}. A comparison of tetracycline detection using different sensors, including our present work, is presented in Table 1. The results show that the composite electrode ($MnWO_4$/f-CNF/GCE) can detect tetracycline at low concentration with a signal-to-noise ratio (S/N) of 3. The sensing capability of the composite electrode is attributed to the high surface area and porosity of the starting materials ($MnWO_4$ and f-CNF). The crystallite sites available in $MnWO_4$ also increase the possibility of tetracycline oxidation, thus allowing low detection limits. The developed modified electrode performed better than the many modified electrodes employed previously for detection of tetracycline in terms of linearity and detection limits.

6. Chronoamperometric Measurements

Chronoamperometric (CA) measurements were performed to

verify the results obtained using the DPV method. Chronoamperometry was performed at various potentials, i.e., 0.4, 0.5, 0.6, and 0.7 V (as shown in Fig. S5 in the SI). The response showed that at 0.6 V, the current was stable and higher than at other potentials. This technique has also been employed to conduct interference studies on tetracycline. We also carried out CA measurements using various concentrations of tetracycline, and the results were consistent with that of the DPV measurements.

7. Reproducibility and Repeatability Studies

Reproducibility and repeatability studies were performed using the modified electrode in the presence of 100 μM tetracycline; the results are shown in Figs. 6(a) and 6(b), respectively. The reproducibility of the DPV response of four different electrodes was tested with 100 μM tetracycline. The DPV curves are superimposable, with only slight variations in current, suggesting that the developed electrode is suitable to detect tetracycline effectively. In addition, the repeatability of the $MnWO_4$/f-CNF/GCE-modified electrode was tested in the presence of 100 μM tetracycline, and a clear current response was obtained with almost no variation among the respective DPV measurements. To check the response of the electrode, repeatability studies were carried out just after adding the analyte, with a 10 s response time for all additions. There was a slight increase in the current measured at the second, third, and fourth measurements as compared to the first measurement. The increase may be attributed to the accumulation of the analyte on the electrodes (the electrode was not replaced during the measurements), which remained constant after the first measurement.

8. Effect of Interfering Agents

Fig. 7 shows the results of tetracycline detection in the presence of interferents amoxicillin, ciprofloxacin, and penicillin. Chronoamperometry, with the potential optimized at 0.6 V, was used to study the effect of the interferents. A 10-μL aliquot of tetracycline was added to the modified electrode, followed by the addition of 10 μL of penicillin (Pen), amoxicillin (Amox), and ciprofloxacin

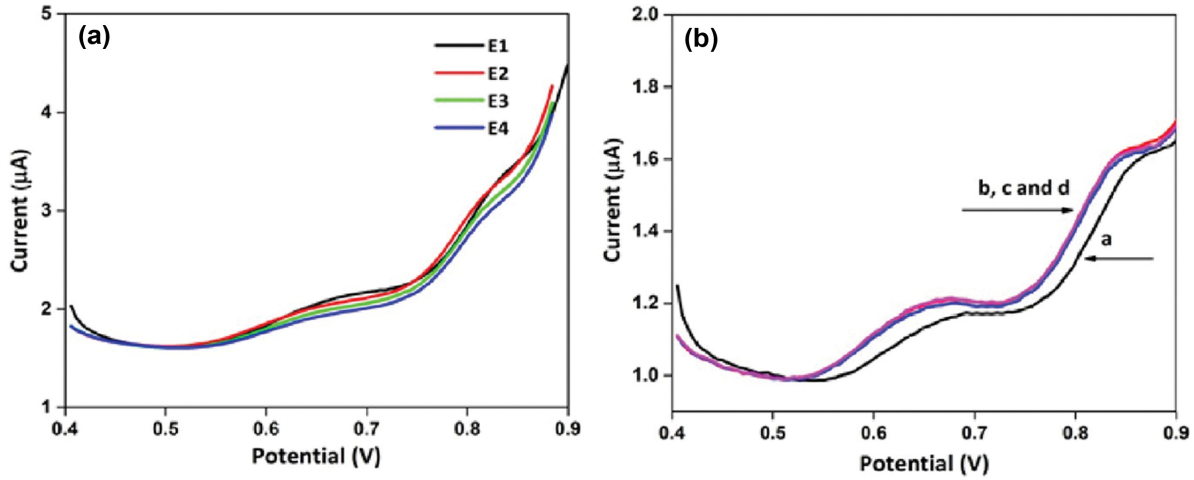

Fig. 6. (a) Reproducibility of differential pulse voltammograms for $MnWO_4$/f-CNF/GCE-modified electrodes (four different electrodes: E1, E2, E3, and E4) in the presence of 100 μM tetracycline. (b) Repeatability of differential pulse voltammograms of $MnWO_4$/f-CNF/GCE-modified electrodes (four different times: a, b, c, and d) in the presence of 100 μM tetracycline.

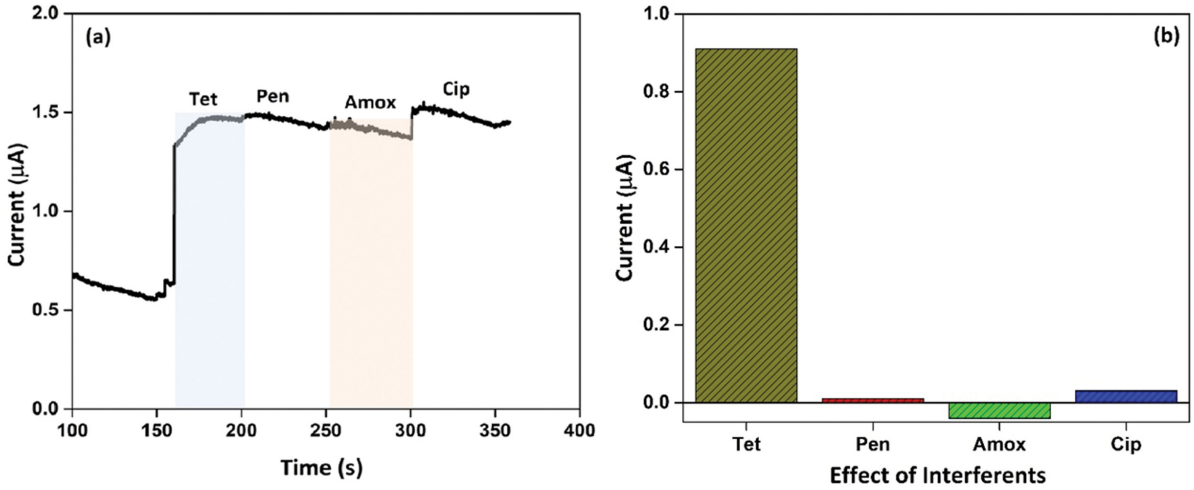

Fig. 7. Effect of interferents (10 μM each of penicillin, amoxicillin, and ciprofloxacin) on the detection of 10 μM tetracycline using $MnWO_4$/f-CNF/GCE-modified electrode: (a) chronoamperometry data and (b) chart showing the current response of the interferents.

(Cip). The current increased with the addition of tetracycline (Fig. 7(a)). However, with the addition of penicillin and amoxicillin, no significant change in the current was observed, indicating the selectivity of the electrode to tetracycline. Adding 10 μL of ciprofloxacin caused a slight increase in current; however, the current was not stable and decreased to the initial point of addition. The current increase may be due to the oxidation of the ionizable groups of ciprofloxacin at physiological pH. Fig. 7(b) shows the current obtained for the analyte tetracycline (Tet) and interferents (Pen, Amox, and Cip) at a potential of 0.6 V. The selectivity of the $MnWO_4$/f-CNF/GCE electrode towards Tet is attributed to the different oxidation potentials of the interferents; for example, the oxidation potential of amoxicillin is 0.81 V [30], that of ciprofloxacin is ~1 V (at BDD) [31], and that of penicillin is ~0.2 V. Hence, at the chosen potential, the interferents have very little effect.

CONCLUSIONS

$MnWO_4$ wafers were successfully synthesized using a facile hydrothermal method. The structural, morphological, and electrochemical properties of the active materials were analyzed using XRD, FTIR, FE-SEM, and electrochemical measurements. The as-synthesized $MnWO_4$ and acid-functionalized CNFs were then made into an ink and drop-casted onto glassy carbon electrodes to sense tetracycline. The sensor exhibited a low detection limit for tetracycline with a wide linear range. This sensor functions optimally in neutral pH (PBS, pH 7), unlike other sensors that work in acidic pH. Also, the sensor exhibits good selectivity towards similar compounds such as Penicillin, Amoxicillin and Ciprofloxacin. Hence, the present sensor can be effectively employed to sense tetracycline in the food and pharmaceutical industries.

ACKNOWLEDGEMENTS

This work was supported by the Priority Research Centers Program through the National Research Foundation of Korea (NRF) funded by the Ministry of Education (grant number 2014R1A6 A1031189) and the 2020 Yeungnam University Research Grant.

AUTHOR CONTRIBUTIONS

Conceptualization, R.R.; methodology, R.R and G.D.; software, R.R and G.D.; validation, R.R.; formal analysis, R.R.; investigation, R.R.; resources, J.J.S.; data curation, R.R.; writing—original draft preparation, R.R.; writing—review and editing, W.K.K.; visualization, R.R.; supervision, J.J.S. and W.K.K.; project administration, W.K.K.; funding acquisition, W.K.K. All authors have read and agreed to the published version of the manuscript.

CONFLICT OF INTEREST

The authors declare no conflict of interest.

ABBREVIATIONS

Amox : amoxicillin
Cip : ciprofloxacin
FTIR : Fourier-transform infrared
f-CNF : functionalized carbon nanofibers
GCEs : glassy carbon electrodes
Pen : penicillin
SEM : scanning electron microscopy
XRD : X-ray diffraction

SUPPORTING INFORMATION

Additional information as noted in the text. This information is available via the Internet at http://www.springer.com/chemistry/journal/11814.

REFERENCES

1. T. Jing, Y. Wang, Q. Dai, H. Xia, J. Niu, Q. Hao, S. Mei and Y. Zhou, *Biosens. Bioelectron.*, **25**, 2218 (2010).
2. I. Chopra and M. Roberts, *Microbiol. Mol. Biol. Rev.*, **65**, 232 (2001).
3. W. D. Welch, R. K. Porschen and B. Luttrell, *Antimicrob. Agents Chemother.*, **24**, 432 (1983).
4. K. N. Agwuh and A. MacGowan, *J. Antimicrob. Chemother.*, **58**, 256 (2006).
5. X. Li, T. Lunkenbein, J. Kröhnert, V. Pfeifer, F. Girgsdies, F. Rosowski, R. Schlögl and A. Trunschke, *Faraday Discuss.*, **188**, 99 (2016).
6. V. Ramasamy Raja, A. Karthika, A. Suganthi and M. Rajarajan, *J. Sci. Adv. Mater. Devices*, **3**, 331 (2018).
7. H. Eranjaneya, P. S. Adarakatti, A. Siddaramanna, P. Malingappa and G. T. Chandrappa, *Mater. Sci. Semicond. Process.*, **86**, 85 (2018).
8. Q. Zou, R. Tang, H. X. Zhao, J. Jiang, J. Li and Y. Y. Fu, *ACS Appl. Nano Mater.*, **1**, 101 (2018).
9. K. L. Klein, A. V. Melechko, T. E. McKnight, S. T. Retterer, P. D. Rack, J. D. Fowlkes, D. C. Joy and M. L. Simpson, *J. Appl. Phys.*, **103**, 061301 (2008).
10. S. Ghosh, W. D. Yong, E. M. Jin, S. R. Polaki, S. M. Jeong and H. Jun, *Korean J. Chem. Eng.*, **36**, 312 (2019).
11. Y. Yang, R. Fu, J. Yuan, S. Wu, J. Zhang and H. Wang, *Microchim. Acta*, **182**, 2241 (2015).
12. H. Faghihian, M. Kooravand and H. Atarodi, *Korean J. Chem. Eng.*, **30**, 357 (2013).
13. M. Rzepka, E. Bauer, G. Reichenauer, T. Schliermann, B. Bernhardt, K. Bohmhammel, E. Henneberg, U. Knoll, H. E. Maneck and W. Braue, *J. Phys. Chem. B*, **109**, 14979 (2005).
14. R. T. Kushikawa, M. R. Silva, A. C. D. Angelo and M. F. S. Teixeira, *Sensors Actuators, B Chem.*, **228**, 207 (2016).
15. H. Wang, H. Zhao, X. Quan and S. Chen, *Electroanalysis*, **23**, 1863 (2011).
16. Y. Yan, J. H. Liu, R. S. Li, Y. F. Li, C. Z. Huang and S. J. Zhen, *Anal. Chim. Acta*, **1063**, 144 (2019).
17. W. Li, J. Zhu, G. Xie, Y. Ren and Y. Q. Zheng, *Anal. Chim. Acta*, **1022**, 131 (2018).
18. R. Ramkumar and M. V. Sangaranarayanan, *ChemistrySelect*, **4**, 9776 (2019).
19. Y. Chen, C. Hu, J. Qu and M. Yang, *J. Photochem. Photobiol. A Chem.*, **197**, 81 (2008).
20. V. Sannasi and K. Subbian, *Ceram. Int.*, **46**, 15510 (2020).

21. M. Daturi, G. Busca, M. M. Borel, A. Leclaire and P. Piaggio, *J. Phys. Chem. B*, **101**, 4358 (1997).
22. L. Zhang, L. Zhang, M. Wan and Y. Wei, *Synth. Met.*, **156**, 454 (2006).
23. C. Liang, W. Xia, H. Soltani-Ahmadi, O. Schlüter, R. A. Fischer and M. Muhler, *Chem. Commun.*, **2**, 282 (2005).
24. X. Chen, G. Zhang, L. Shi, S. Pan, W. Liu and H. Pan, *Mater. Sci. Eng. C*, **65**, 80 (2016).
25. H. Filik, A. A. Avan, S. Aydar, D. Ozyurt and B. Demirata, *Curr. Nanosci.*, **12**, 527 (2015).
26. C. M. F. Calixto, P. Cervini and É. T. G. Cavalheiro, *Int. J. Environ. Anal. Chem.*, **92**, 561 (2012).
27. W. R. Chen and C. H. Huang, *Environ. Pollut.*, **159**, 1092 (2011).
28. S. Muthamizh, R. Suresh, K. Giribabu, R. Manigandan, S. Praveen Kumar, S. Munusamy and V. Narayanan, *J. Alloys Compd.*, **619**, 601 (2015).
29. R. K. Devi, G. Muthusankar, S. M. Chen and G. Gopalakrishnan, *Microchim. Acta*, **188**, 196 (2021).
30. L. Devkota, L. T. Nguyen, T. T. Vu and B. Piro, *Electrochim. Acta*, **270**, 535 (2018).
31. G. S. Garbellini, R. C. Rocha-Filho and O. Fatibello-Filho, *Anal. Methods*, **7**, 3411 (2015).
32. A. Benvidi, S. Yazdanparast, M. Rezaeinasab, M. D. Tezerjani and S. Abbasi, *J. Electroanal. Chem.*, **808**, 311 (2018).
33. H. Guo, Y. Su, Y. Shen, Y. Long and W. Li, *J. Colloid Interface Sci.*, **536**, 646 (2019).
34. Y. J. Kim, Y. S. Kim, J. H. Niazi and M. B. Gu, *Bioprocess Biosyst. Eng.*, **33**, 31 (2010).
35. A. Wong, M. Scontri, E. M. Materon, M. R. V. Lanza and M. D. P. T. Sotomayor, *J. Electroanal. Chem.*, **757**, 250 (2015).
36. T. Gan, Z. Shi, J. Sun and Y. Liu, *Talanta*, **121**, 187 (2014).
37. A. Olugbenga Osikoya and P. Poomani Govender, *Electroanalysis*, **33**, 412 (2021).
38. K. Yang, P. Jia, J. Hou, T. Bu, X. Sun, Y. Liu and L. Wang, *ACS Sustain. Chem. Eng.*, **8**, 17185 (2020).
39. Y. Yang, H. Huang, X. Wang, L. Zhang, A. Hao, Z. Shi and C. Dai, *ACS Appl. Nano Mater.*, **3**, 9796 (2020).
40. J. Guo, W. Lu, H. Zhang, Y. Meng, F. Du, S. Shuang and C. Dong, *Sensors Actuators, B Chem.*, **330**, 129360 (2021).
41. Y. Zhang, M. Lv, P. Gao, G. Zhang, L. Shi, M. Yuan and S. Shuang, *Sensors Actuators, B Chem.*, **326**, 129009 (2021).

Supporting Information

Differential pulse voltammetric sensor for tetracycline using manganese tungstate nanowafers and functionalized carbon nanofiber modified electrode

Ramya Ramkumar, Ganesh Dhakal, Jae-Jin Shim, and Woo Kyoung Kim†

School of Chemical Engineering, Yeungnam University, Gyeongsan, Gyeongbuk 38541, Korea
(*Received 16 November 2021 • Revised 15 December 2021 • Accepted 29 December 2021*)

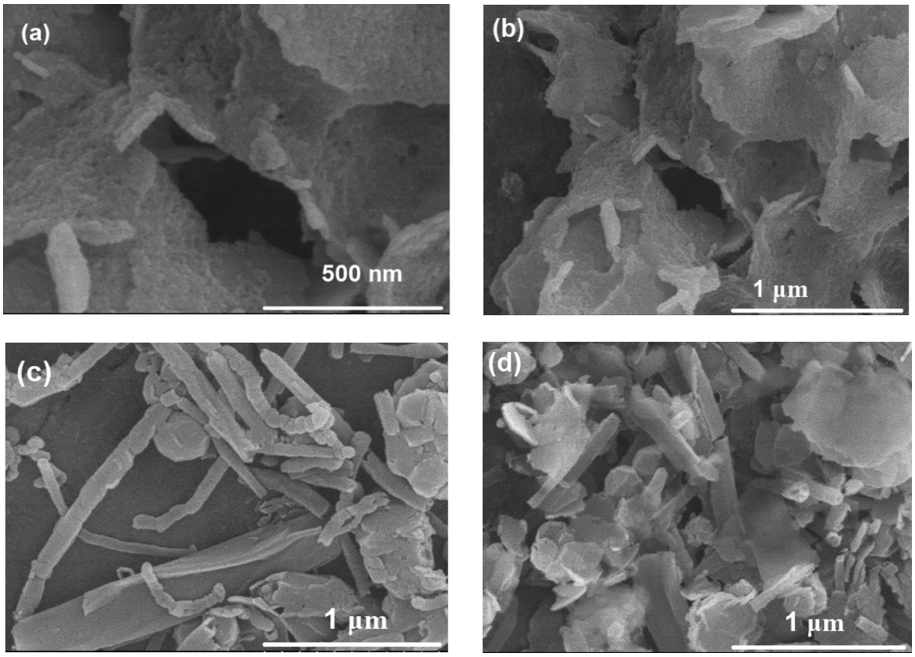

Fig. S1. SEM of (a), (b) $MnWO_4$ (@ 100k and 50k magnification), (c) f-CNF (@ 50k magnification) and (d) $MnWO_4$/f-CNF composite (@ 50k magnification).

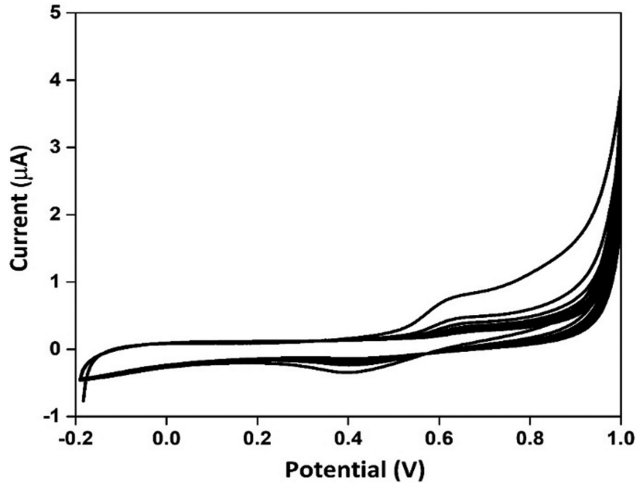

Fig. S2. Cyclic voltammograms of $MnWO_4$/f-CNF/GCE modified electrode stabilization in the presence of PBS 7 at 40 mV s^{-1} for 20 cycles.

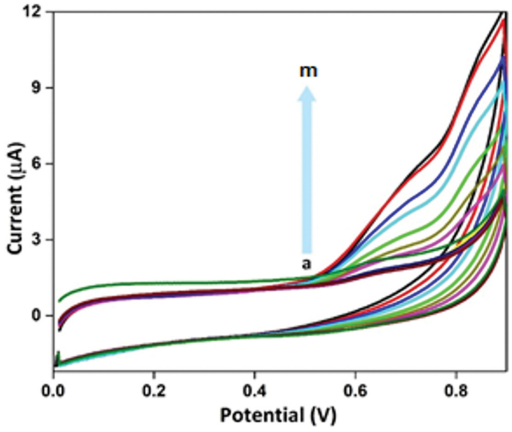

Fig. S3. Cyclic voltammograms of $MnWO_4$/f-CNF/GCE modified electrode in the presence of different concentrations of tetracycline, (a) 0, (b) 1.75, (c) 4.25, (d) 9.25, (e) 19.25, (f) 39.25, (g) 69.25, (h) 109.25, (i) 159.25, (j) 209.25, (k) 259.25, (l) 309.25, and (m) 359.25 µM, respectively.

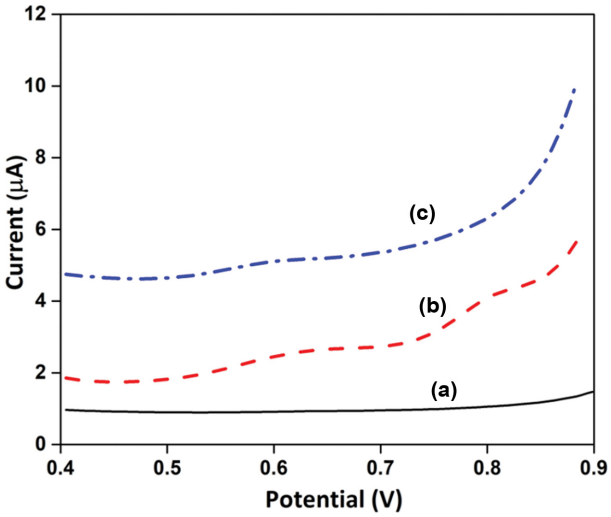

Fig. S4. Differential pulse voltammograms for $MnWO_4$/f-CNF/GCE-modified electrode at different pulse amplitudes of (a) 10, (b) 25, and (c) 50 mV in the presence of 100 μM tetracycline.

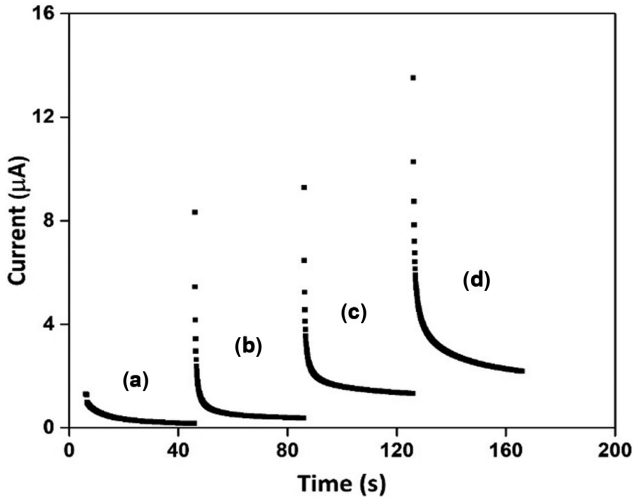

Fig. S5. Chronoamperometric curves at different potentials (a) 0.4, (b) 0.5, (c) 0.6 and (d) 0.7 V for $MnWO_4$/f-CNF/GCE modified electrode in the presence of 100 μM of tetracycline.

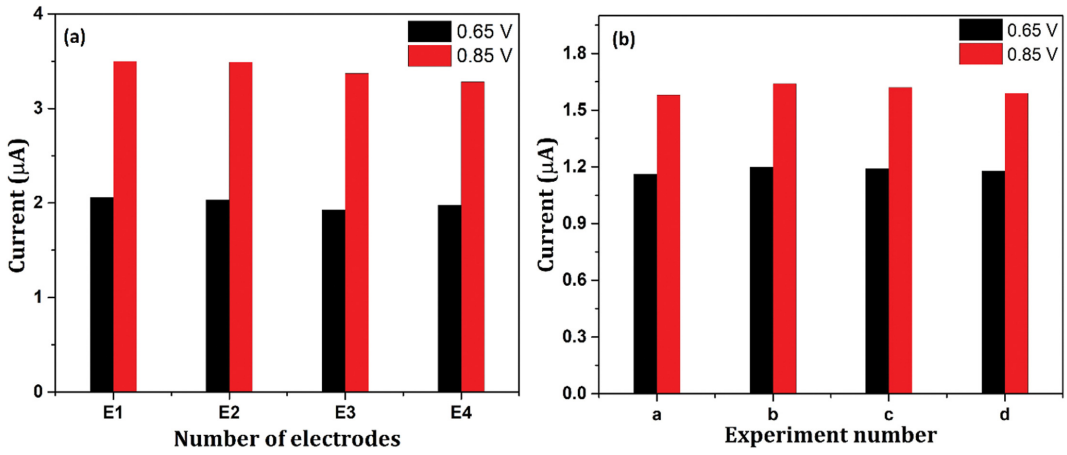

Fig. S6. (a) Bar graph showing the reproducibility of differential pulse voltammograms for $MnWO_4$/f-CNF/GCE-modified electrodes (four different electrodes: E1, E2, E3, and E4) in the presence of 100 μM tetracycline. (b) Bar graph showing the repeatability of differential pulse voltammograms of $MnWO_4$/f-CNF/GCE-modified electrodes (four different times: a, b, c, and d) in the presence of 100 μM tetracycline.